Modeling Power Loss Due to Wind Turbine Icing

Davis, Neil; Hahmann, Andrea N.; Clausen, Niels-Erik; Zagar, Mark

Publication date:
2014

Modeling Power Loss Due To Wind Turbine Icing

Neil Davis1,2, Andrea Hahmann 1, Niels-Erik Clausen 1, Mark Zagar 2

1: DTU Wind Energy; 2: Vestas Technology R&D Aarhus, DK

Acknowledgements: This work is funded by the Top-Level Research Initiative (TFI) project, Improved forecast of wind, waves and icing (IceWind) and Vestas.

Introduction

Figure 1. Photo illustrating Ice shedding & accretion on a turbine in Grenchenbuerg Sweden (Lasko et al, 2010).

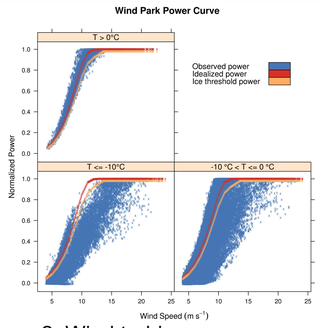

Figure 2. Wind turbine power curve at different air temperatures. The deviation from the power curve at colder temperatures is believed to be the result of icing.

The growth of ice on a wind turbine can pose it many problems. Icing can create a potential safety risk due to ice shedding (fig. 1), lead to production losses which reduce profits (fig. 2), and can increase loads, thereby reducing the turbine lifetime.

Icing Forecast System

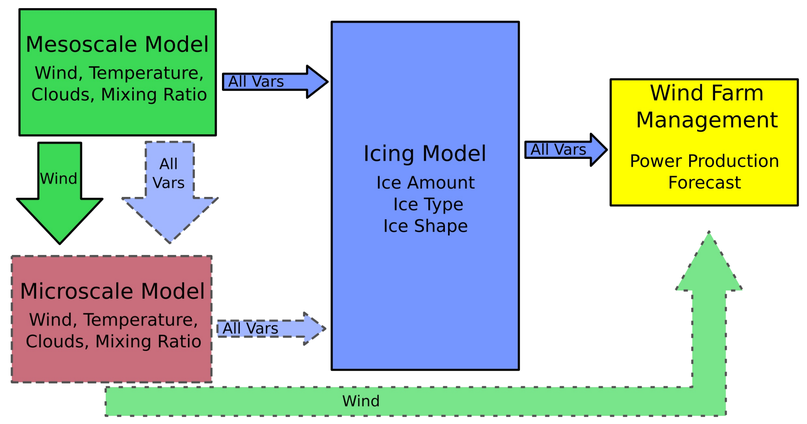

Figure 3. Illustration of a wind turbine power forecasting system which includes icing.

Green objects: Pre-existing
Yellow objects: Updated for icing
Red objects: Need update for icing
Blue objects: New for icing model

Dashed lines signify items still in need of development / updating.

The ability to forecast turbine icing and model expected power losses (fig. 3) could help to minimize risks both by identifying sites prone to icing during the planning phase, and estimating production losses in the short term.

Icing Model

$$\frac{dM}{dt} = \alpha_1 \alpha_2 \alpha_3 \omega v A$$

Equation 1. Makkonen Equation for Ice Mass, ω is the liquid water content, and v is the wind speed, A is the cross sectional area. The α terms are efficiency terms. For liquid icing, α2 is set to 1.

Ice Accretion: Growth of ice, function of the heat balance between the heat released via the phase change and other parameters.

Fig. 4 highlights α_1, function of wind speed, droplet size and cylinder diameter. For turbine icing wind speed is adjusted based on RPM of the turbine

Fig. 5 shows how colder temperatures are required to freeze ice as more cloud mass contacts the turbine blade (α_3).

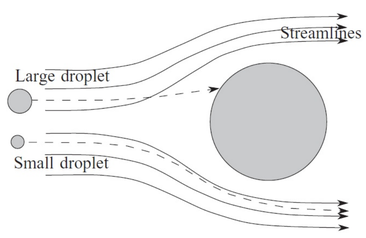

Figure 4. Trajectory of different sized droplets around a cylinder (Makkonen, 2000).

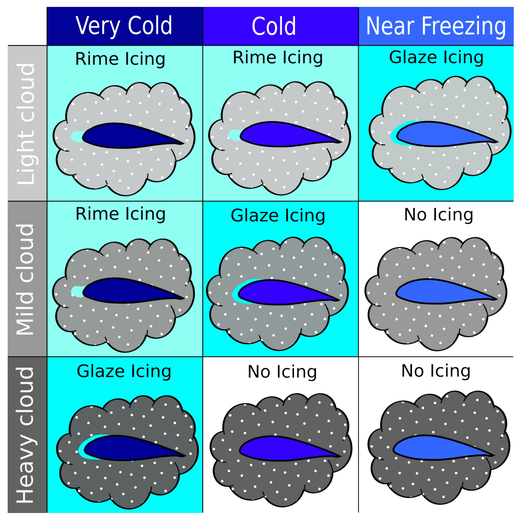

Figure 5. Impact of temperature and mass flux on ice.

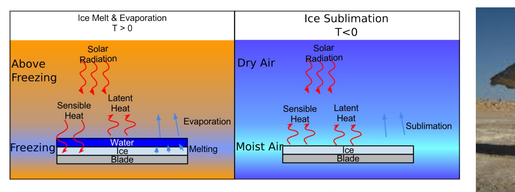

Figure 6. Energy (red) and mass (blue) flows for ice undergoing melting or sublimation.

Figure 7. Example of wind erosion of rock.

Ice Ablation: Melting/evaporation, sublimation or shedding of ice

iceBlade Model includes sublimation and wind erosion terms. Sublimation is solved by an empirical solution from Srivastava and Coen (1992). Wind erosion term was added as a numerical fit, based on the kinetic energy of the wind.

Total Shedding of ice occurs when the mesoscale model forecasts a temperature above freezing.

Observed Icing

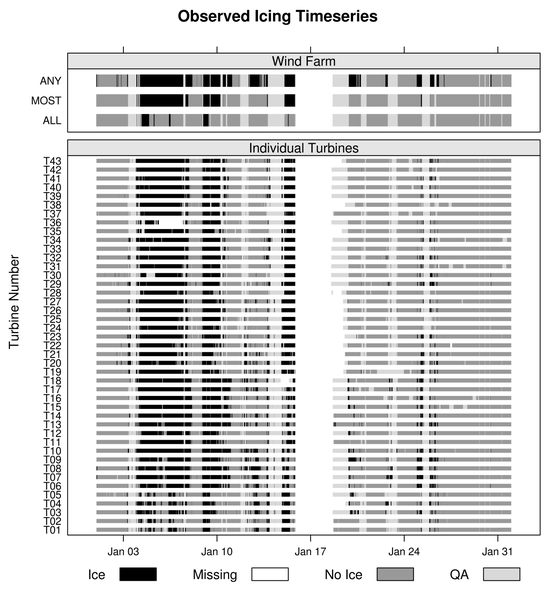

Figure 8. Icing periods for 41 individual turbines, and wind farm icing classes based on how many turbines were iced.

Observed icing has to be infered from the turbine data. The current approach uses the observed power curve and nacelle measurments. Fitting a smooth to the standard deviation of observed power at each 0.1 m/s bin of wind speed, and subtracting that from the empirical power curve of each turbine.

This curve is used as a threshold as shown in fig. 1, and when more than 3 points cross this line with a nacelle temperature less than 3°C, those points are marked as iced.

There is large variation in the amount of icing across the different turbines.

In general we found that most of the turbines experienced the same icing periods, however there were some periods where only a few turbines were iced, particularly at the beginning and end of the period.

Mesoscale Model Comparison

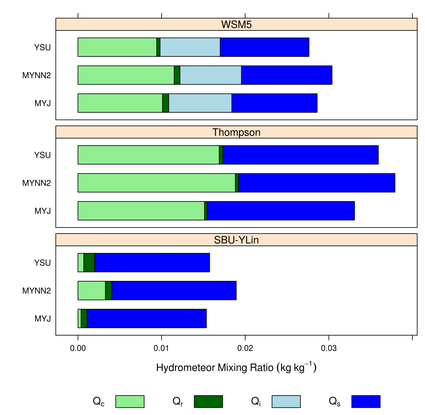

Figure 9. Modeled cloud amounts for sensitivity studies. Qc is liquid cloud water, Qr is rain water, Qi is cloud ice, and Qs is snow.

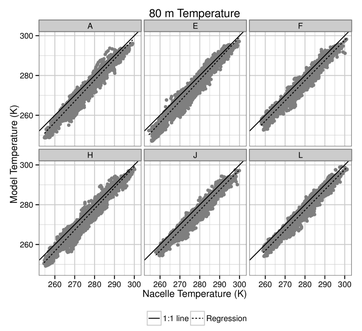

Figure 10. Temperature evaluation at 6 wind parks. Nacelle temperatures are the park mean values.

WRF mesoscale model was run for 9 sensitivity tests with a matrix of 3 PBL schemes and 3 microphysics schemes.

Fig. 9 shows the impact of these schems on the cloud hydrometeors. The precipiation was almost equal across the schemes, so it cannot be used to determine which scheme is optimal. The Thompson microphysics scheme had the most liquid cloud water content, which suggests it is best representing super-cooled clouds.

Temperature analysis in fig. 10, shows WRF has a large cold bias especially at colder temperatures.

iceBlade evaluation

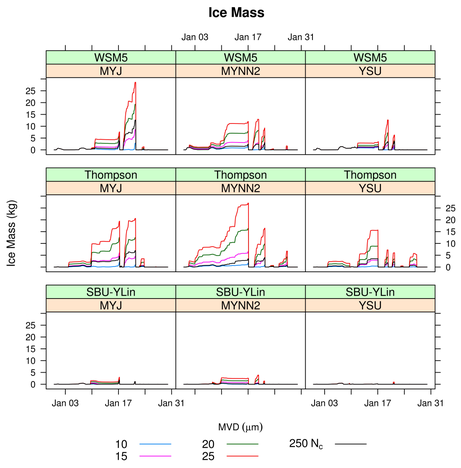

Figure 11. Timeseries of ice mass for different WRF sensitivities. MVD values were constant for 5, 10, 15, and 20 curves, while they were calculated using a cloud particle count of 250 in the black curve.

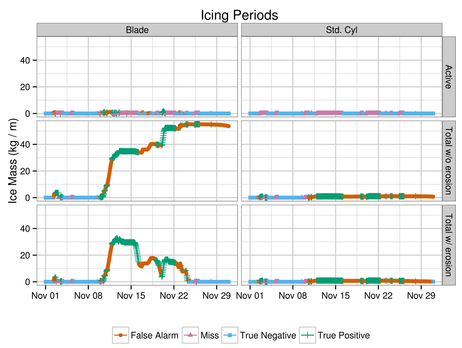

Figure 12. Timeseries of ice mass at a wind park showing the impact of the wind erosion term. Colors highlight how the model compares with the obsered icing signal.

Figure 11 shows that the SBU-YLin scheme produces very little ice mass compared to the other two schemes, which is largely due to the limited amount of cloud water from that parameterization. The Thompson scheme generally shows the most ice.

The different prescribed MVD values show large variation in the amount of ice, but the two largest droplet sizes show very similar durations. The calculated MVD tends to have ice mass lower than the prescribed value of 15 microns. This is expected as the MVD varies with cloud amount in the calculated value.

Figure 12 shows the impact of the wind erosion term, which greatly reduces the ice mass for the second half of November. This term is key for long term simulations of icing.

During cold temperatures very little ice is removed, compared to the growth rate of the ice, while most of the ice is removed via the 100% shedding method used when temperatures were above freezing.

Power Loss Model

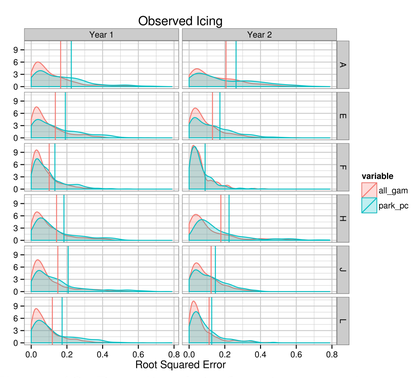

Figure 13. Density plot of root squared error for times with observed icing, comparing the unadjusted park power curve (park_pc) and the power curve with modeled power loss (all_gam). Vertical lines are the RMSE.

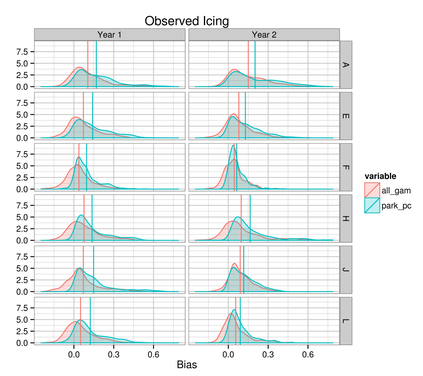

Figure 13. Same as figure 12, but for model bias for the density, and mean bias for the vertical lines.

The Power loss model was created as a hierarchical model, splitting the data-set into two pieces depending on if ice was forecast or not. Then each split was modeled using a generalized additive model.

The ice side of the model, shown in figures 13 & 14, had the WRF wind speed, accreted ice, and accumulated ice as its inputs. The GAM model was fit for year 1, using data from all 6 wind parks. The year 2 results are the model prediction based on the previous fit.

The model improves both the bias and error estimates at most wind farms. The largest change can be seen in the bias plot, where several of the large over predicted values in the unadjusted estimate are removed, and there is a larger spread of negatively biased values.

An additional sensitivty was run where each park was fit indivually and this method tended to result in the overfitting of the model, likely due to the lack of icing events in a given year.

References

Cattin, R., S. Kunz, A. Heimo, G. Russi, M. Russi, and M. Tiefgraber, 2007: Wind turbine ice throw studies in the Swiss Alps. European Wind Energy Conference Milan, Vol. 1 of, 3–7.

Laakso, T. and Coauthors, 2010: State-of-the-art of wind energy in cold climates. VTT, Finland,.

Makkonen, L., 2000: Models for the growth of rime, glaze, icicles and wet snow on structures. Philosophical Transactions of the Royal Society of London. Series A: Mathematical, Physical and Engineering Sciences, 358, 2913–2939.

Srivastava, R.C. & Coen, J.L., 1992. New Explicit Equations for the Accurate Calculation of the Growth and Evaporation of Hydrometeors by the Diffusion of Water Vapor. Journal of the Atmospheric Sciences, 49(17), pp.1643–1651.

Davis, N. et al., 2014. Forecast of Icing Events at a Wind Farm in Sweden. Journal of Applied Meteorology and Climatology, 53(2), pp.262–281.